

Energy-based Structure Prediction for $d(\text{Al}_{70}\text{Co}_{20}\text{Ni}_{10})$

Nan Gu^{†‡}, M. Mihalkovič^{†§}, and C. L. Henley[†]

[†] Dept. of Physics, Cornell University, Ithaca NY 14853-2501, USA

[‡] Present address: Dept. of Physics, M.I.T., Cambridge MA 02139 [CORRECT THIS]

[§]Permanent address: Institute of Physics, Slovak Academy of Sciences, 84228 Bratislava, Slovakia.

Abstract. We use energy minimization principles to predict the structure of a decagonal quasicrystal - $d(\text{AlCoNi})$ - in the Cobalt-rich phase. Monte Carlo methods are then used to explore configurations while relaxation and molecular dynamics are used to obtain a more realistic structure once a low energy configuration has been found. We find five-fold symmetric decagons 12.8Å in diameter as the characteristic formation of this composition, along with smaller pseudo-five-fold symmetric clusters filling the spaces between the decagons. We use our method to make comparisons with a recent experimental approximant structure model from Sugiyama et al (2002).

PACS numbers: 61.44.Br, 61.50.Lt, 61.66.Dk, 64.60.Cn

1. Introduction

This paper reports structural predictions for the decagonal quasicrystal $d(\text{AlCoNi})$ in the Cobalt-rich ('basic Co') phase, of approximate composition $\text{Al}_{70}\text{Co}_{20}\text{Ni}_{10}$ and atomic density $0.068 \text{ atoms}/\text{\AA}^3$, using simulations to minimize energy, using the same methods (and codes) as previous papers by Mihalkovic, Widom, and Henley [1, 2, 3] on the 'Ni-rich' phase; this constitutes a first test of the transferability of that approach to other compositions that are described by other tiling geometries.

The Aluminum-Nickel-Cobalt alloy $d(\text{AlCoNi})$ is the best studied and perhaps the highest quality of equilibrium decagonal quasicrystals. Decagonal $d(\text{AlCoNi})$ has about eight modifications (which we call 'phases' here), each existing in a tiny domain of the phase diagram.[4, 7, 5, 6, 8]. The compositions 'basic Ni' (around $\text{Al}_{70}\text{Co}_{10}\text{Ni}_{20}$), and 'basic Co' are the best-studied phases, having the simplest diffraction patterns. (The other phases show superstructure peaks, indicating modulations.) Several crystal approximants related to 'basic Co' are known [9], one of which has a solved structure [10].

We find that (in contrast to the 'basic Ni' phase), the framework of 'basic Co' at $T = 0$ is a network of edge-sharing 12.8Å diameter decagons (placed like the large atoms in a "binary tiling" quasicrystal). A strong (but not always simple) Co/Ni ordering is found. Our model reproduces most, but not all, of the atomic positions in $W(\text{AlCoNi})$. (A complementary brief account of our results is in Ref. [11], and a more complete account is in preparation [12].)

2. Methods

Our main assumption is that the $d(\text{AlCoNi})$ structure is well approximated by a stacking of equally spaced two-dimensional tilings built from the Penrose rhombi under periodic boundary conditions. The chief experimentally determined inputs were the values $c = 4.08\text{\AA}$ for the stacking period and $a_0 = 2.45\text{\AA}$ for quasilattice constant (edge length of small rhombi). It should be noted that the actual period for the Co-rich phase is generally believed to be $2c$; we used c because (i) it is the simplest starting point, and was used in the prior study of the Ni-rich phase [1, 2] (ii) so long as the atoms are fixed on discrete sites (see Section 3), it turns out that period c is optimal even when a cell with more layers is allowed; (iii) even in our final, relaxed period $2c$ structure (Section 4), most atoms do repeat with period c .

This framework of decorated tilings takes advantage of the fact that all the known atomic structures of decagonals are Penrose-tiling-like. Further, even in random tilings Penrose rhombi admit “inflation” constructions that can relate a tiling to another one using rhombi with edges enlarged by $\tau = (1 + \sqrt{5})/2 \approx 1.618$ (the golden ratio), which gives a convenient way to build a chain of connections from the atomic level to large tiles so as to describe $d(\text{AlNiCo})$ on large scales. Fig. 1 includes two ways of subdividing a unit cell into a tiling of rhombi (with edges a_0 and τa_0 , respectively).

We also assume atomic pair potentials between Al, Co, and Ni as derived *ab initio* using Generalised Pseudopotential Theory [13] (GPT), but modified using results from *ab initio* calculations to approximate the sums of the omitted many-body interactions when transition metals (TM) are nearest neighbours. [Fig. 1 of Ref. [1] plots these potentials.] The potentials are cut off by a smooth truncation past 7.0\AA .

We know [1, 2] that the strongest interaction is the Al-TM first potential well. The number of Al-TM neighbours is maximised and, as a corollary, that of TM-TM nearest neighbours is minimised (but TM-TM second neighbours, at $\sim 4\text{\AA}$ separation, are common). However, this scarcely constrains the structure since the weak Al-Al potential allows enormous freedom in placing Al. In practice, one finds in Al-TM quasicrystals that a rather rigid TM-TM network forms, with separations near to the strong second minimum of the TM-TM pair potential; the Al atoms fill the TM interstices in a more variable fashion. Subtle details of the density and composition, as well as the small differences between Co and Ni in the pair potentials, decide which structure optimises the energy. We understand only a few of these factors in detail for the ‘basic Co’ phase, so in this paper we will only describe the atomic structures we found and do not attempt a microscopic rationalization of them.

Our program uses Metropolis Monte Carlo (MMC) simulation to perform atom-atom and atom-vacancy swaps within a site list placed on the Penrose tiles. The first stage simulations include an additional degree of freedom in the form of ‘tile flips.’ These ‘tile flips’ obey the MMC algorithm probabilities and conserve tile number, atomic species number, and the collective outline of tiles rearranged.

Our procedure is to anneal from a high temperature $\beta \approx 4\text{--}10\text{ eV}^{-1}$ to a low temperature at which most degrees of freedom are frozen out, $\beta \approx 20\text{ eV}^{-1}$, using a step size $\delta\beta \approx 0.5\text{--}1\text{ eV}^{-1}$. (Here $\beta \equiv (k_B T)^{-1}$.) At each temperature step,

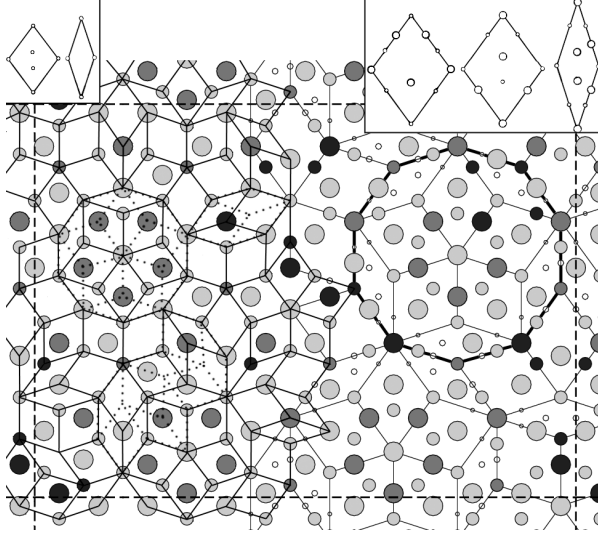


Figure 1. The $32 \times 23 \times 4$ unit cell. The left half is subdivided into a_0 scale rhombi (in two ways in part of the cell [dotted lines]). The right half of the cell is subdivided into τa_0 scale rhombi. The atomic configuration shown was obtained from the τa_0 scale simulation. (The atomic locations are also valid for the a_0 scale decoration, but configurations from a_0 scale simulations almost always have more defective occupations.) Insets at top left and top right display the candidate sites on the a_0 and τa_0 scale tiles, respectively. Filled large circles depict atoms in one layer and filled small circles are those in the other layer. Black denotes Nickel, dark gray Cobalt, and light gray Aluminium. Unoccupied sites of the τa_0 scale tiling are shown by very small empty circles; those of the a_0 scale tiling are not shown. Four 13Å Decagon motifs (described in Sec. 3.1) are present: e.g. one is seen decomposed into ten τa_0 edge rhombi near the cell's upper right corner.

approximately 2000 atomic swaps per site are attempted.

2.1. Multiscale Procedure

The strategy of our series of simulations loosely copies that reported previously [1, 2] on the Ni-rich phase of $d(\text{AlNiCo})$, and can be thought of as a sort of multiscale modelling. It proceeds in the following stages:

1. Begin with Monte Carlo simulations allowing atom swaps and ‘tile-flips’ with a tiling of relatively small Penrose rhombi; note prominent features and formations that recur in all the low energy structures from a sufficient number of independent runs.
2. Take the observations from the small-scale tiling and promote them to rules: i.e. make the formations inferred in the first stage into fundamental objects of a larger scale tiling. Unused (or underused) degrees of freedom are removed.
3. Perform new Monte Carlo simulations on the larger-scale tiling to search for

new low energy structures. This larger- scale tiling is generally more efficient at finding lower energies because of the reduced degrees of freedom.

4. Verify that the degrees of freedom removed in stage (2) were indeed unnecessary by restoring some of them, judiciously.
5. Repeat for larger and larger scale tilings. An eventual goal is to extract a ‘tile Hamiltonian’ [14, 15] which is the bridge to modelling long-range order and diffuse scattering. That means ascribing the atom-atom energies to an effective interaction among neighbouring tiles, so that tiles are the only remaining degree of freedom.

It is also necessary to perform relaxations/molecular dynamics to escape the biases which may be introduced by the discrete site list used up through stage (4).

3. Results

3.1. Small-Scale tiling (edge $a_0 = 2.45\text{\AA}$)

The first stage of our tiling simulations uses small Penrose rhombi that have $a_0 = 2.45\text{\AA}$ edges. The unit cell simulations had dimensions $32.01\text{\AA} \times 23.25\text{\AA} \times 4.08\text{\AA}$, which we shall call the $32 \times 23 \times 4$ cell, shown in Fig. 1. The structure is taken to repeat after two layers of the Penrose tiling. At $0.068 \text{ atoms/\AA}^3$, there are about 200 atoms in the unit cell.

Our low energy configuration generated at this level showed distinct rings of 5 TM and 5 Al atoms surrounding an Al atom and surrounded by an 10 Al atom decagon with an edge length of a_0 . These 21-atom motifs were evidently energy favourable. Linear regressions of the count of these 21-atom clusters versus energy revealed a noisy, but consistent correlation of $\approx -1.0 \text{ eV}$ per 21-atom cluster.

However, the ideal structure did not simply maximize the number of 21-atom clusters: though they may be placed adjacent to pack six clusters per cell, that was typically not observed in the low-energy configurations. Instead, further MMC annealing (starting from a low-energy configuration) found that a larger cluster emerged as the characteristic motif at this composition: a decagon with an edge length of $\tau a_0 \approx 4.0\text{\AA}$ (hence a diameter of $\sim 12.8\text{\AA}$), which we will call ‘ 13\AA Decagon’ (13\AA D). This object contains the 21-atom motif at its centre, ten TM atoms at its vertices, and Al atoms irregularly interspersed along and within its edges.

We use the following nomenclature for the components of 13\AA D , from its centre outwards. The centre of the 13\AA D is an Al atom. The 5 TM 5 Al ring is known as the ‘first ring.’ The TM atoms in the first ring are in the same layer as the central Al atom. The 10 Al ring is known as the ‘second ring.’ The 10 TM decagon and the Al atoms along and within the edges are collectively known as the ‘third ring.’ Miscellaneous Al sites occur between the second and third rings, which we designate collectively as the ‘2.5 ring.’

In the 13\AA D , the first ring TM sites are mainly occupied by Co and the third ring (decagon vertex) TM sites also tend to Co occupation, but there is a very strong dependence on the local environment that distinctly favour Ni in certain sites. [This

became clear at the second stage of simulation, Subsec. 3.2.] The Al positions of third-ring and 2.5 ring Al atoms are closely correlated and the rules were not resolved from the 2.45\AA tiling simulation.

A second type of motif fills the interstices between the 13\AA Ds: it consists of a 10-atom ring and an Al at the centre, much like ring 1 in the 13\AA D cluster, except this kind of motif has mixed Al-TM occupations for the 5 candidate TM sites. In general, about 3 sites out of the 5 candidates are filled with TM atoms, preferably Ni. We name these 11-atom clusters “Star clusters”; a few of these are contained in Fig. 1.

Perfect examples of either cluster were rarely observed in the first (2.45\AA) level of simulation: their decorations were induced by a ‘consensus’ or average over many defective examples. Thus, the rules for Al/TM occupation on the Star cluster TM sites, and for Ni/Co occupation on all TM sites, were still incompletely known from this stage.

3.2. Inflated Tiling ($\tau^3 a_0 \rightarrow \tau a_0$)

In keeping with our ‘multiscale’ methodology, we reassessed the degrees of freedom necessary for the next level of simulation. The dominant geometric object is a decagon with edge $\tau a_0 \approx 4\text{\AA}$, but we found it economical to represent its decoration by candidate sites using a thin 4\AA rhombus and the second fat rhombus shown in the right inset of Fig. 1; similarly, the Star cluster decoration is represented using the first fat rhombus.

We assumed that the minimum-energy structure has a maximum density of 13\AA D clusters. A Monte Carlo simulation was carried out (admitting only tile flips) on the ensemble of τa_0 rhombus tilings using an artificial tile Hamiltonian favouring the creation of nonoverlapping ‘star decagons’ (of edge τa_0) containing a fivefold star of fat rhombi. ‡ It was found that the ground state configuration was always a ‘binary tiling’ [16, 17] of rhombi with edge length $\tau^3 a_0 = 10.4\text{\AA}$ with the ‘large atom’ and ‘small atom’ vertices replaced by 13\AA Ds and Star clusters, respectively. (The constraints on possible decagon separations imposed by building them from τa_0 tiles are consistent, in fact, with those due to the potentials [12].)

We **designate** a fixed site list on the τa_0 rhombi, as shown in the right half of Fig. 1, designed to match the most frequently occupied sites observed in the low-energy states from out a_0 scale simulations. This tiling, unlike the a_0 tiling, consists of only *one* layer of Penrose tiles, each of which has site decorations in *two* layers spaced 2.04\AA in the c direction. Note how the two versions of the fat Penrose rhombus have different site lists. We use the $32 \times 23 \times 4$ cell, as before so we may compare the energies for systems with exactly the same density and composition.

At this second stage, our MMC runs had purely lattice gas moves on a fixed tiling (no tile flips). These were able to find lower energy configurations at a much faster rate than the first-stage (a_0 scale) simulations at the same composition and atomic density, due to the much decreased site list. Hence, the occupations of many types of sites were discerned with greater accuracy, such as the TM sites in the

‡ Star decagons were similarly maximized in Ref. [18], except they could overlap in that case.

13Å Decagon (already described in Subsec. 3.1). Furthermore the tendencies of more variable sites (Al in rings 2.5 and 3, and TM in the Star cluster), which will be described in a longer paper [12], started to come into focus. Finally, despite having *fewer* allowed configurations, the τa_0 tiling simulation consistently found *lower* energies, which serves as our post hoc justification for assuming 13ÅD clusters in the binary tiling geometry and the reduced site list. §

In the prior case of the ‘basic Ni’ phase, the decoration model [1] was implemented as a deterministic tiling. A marked contrast in the present ‘basic Co’ case is that we cannot impose a simple rule that fixes the chemical occupation of each site. On certain TM sites, it is difficult to resolve the occupation (Co/Ni); certain Al sites are also variably occupied (Al/vacant) depending on the environment. Presumably, with a sufficiently thorough understanding of our model, we could formulate a deterministic decoration rule on the binary tiling. It is possible, however, that the energy differences among some competing structures are too small to be visible in a reasonable simulation, or to influence the real properties at any accessible temperature.

3.3. Cluster orientation

The physical accessible candidate sites in the τa_0 decagons (with our decoration) in fact have a $\overline{10}$ point group symmetry, which is not broken by the binary tiling geometry. The fivefold symmetric 13ÅD cluster breaks this symmetry, by the layer on which the central Al sits and the Al/TM alternation on the first ring. Thus, a major obstacle to writing a deterministic decoration is that the relative orientations of 13ÅDs must be specified, which depends on subtle interaction energies between them. Experimentally, $d(\text{AlCoNi})$ with our Co-rich composition was observed to order in a fivefold symmetry, wherein all the Decagons are oriented the same way [19, 20].

As a test, we compared the lowest-energy configurations resulting from MMC simulations on identical τa_0 tilings in which neighbouring 13ÅDs were forced either to have always identical or always opposite orientations. [This is controlled by the orientation of the decagon of τa_0 rhombi in the tiling that gets decorated.] we evaluated the minimum-energy configurations from ~ 60 independent runs of each type. We used the $32 \times 23 \times 4$ unit cell, using a fixed composition $\text{Al}_{70}\text{Co}_{20}\text{Ni}_{10}$, but repeating the tests for a series of atom number densities n .

The energy difference between these two orientations was density dependent. At $n \approx 0.068$ atoms/Å³ the two orientational patterns are practically degenerate (though with visibly distinct atom configurations.) From $n = 0.068$ Å⁻³ to 0.074 Å⁻³ – a range which includes the most realistic compositions – the pattern with uniform orientations has the lower energy, by up to 4×10^{-3} eV/atom, but this difference disappears again at $n \approx 0.074$ Å⁻³.

We find this energy difference arises from different ways of filling the possible TM sites in the respective orientation schemes. In the uniform-orientation scheme, as

§ In additional tests, certain candidate sites that are absent in the inflated tiling were restored systematically to the τa_0 tiles, and it was verified this had a negligible effect.

the TM density is raised (as part of the total density), TM atoms fill the ring 2.5 in the 13\AA Decagon before they exceed $\sim \frac{3}{5}$ filling in the Star cluster TM sites; whereas in the alternating-orientation case, the ring 2.5 is filled to a lesser degree with TM while the Star cluster TM sites become overfilled. [In Ref. [11], we gave an explanation how these effects could favour *alternating* orientations.] But the results just presented are valid only for the (unphysical!) case of atoms confined to hop on fixed ideal sites. When displacements are allowed, so that many atoms “pucker” away from the flat layers (see Sec. 4), then the uniform arrangement is preferred more robustly.

4. Beyond the Discrete Site List

Up to this point, we reported simulations using fixed atom site positions. We can make our configurations more realistic by subjecting them to relaxation and molecular dynamics (MD). The removal of the tiling and discrete site list leads to effects such as out-of-layer “puckering” and so-called ‘period doubling,’ whereby certain atoms relax into positions that violate the c period of a single unit cell, but instead are periodic with respect to a unit cell with $c' = 2c = 8.16\text{\AA}$. Exactly such distortions are familiar in the structures of decagonal phases and approximants.

Our standard cycle for such ‘off-site’ studies is a relaxation to a local energy minimum (i.e. to 0 K), followed by an MD cycle beginning at ~ 600 K and ending at ~ 50 K in increments of 50 K. The MD results are then relaxed again to 0 K. This protocol will be denoted Relaxation-MD-Relaxation (RMR). Upon relaxation to $T = 0$, we find that the TM atoms are quite immobile and move only slightly. The Al atoms, however are subject to displacements as large as 1.5\AA . After molecular dynamics and re-relaxation to $T = 0$, we find a few Al atoms be further displaced, but to similar sites so that no systematic difference is apparent in the overall pattern.

4.1. Comparison with Experimental W-AlCoNi

Major diffraction-based structure models were available for ‘basic Ni’ $d(\text{AlNiCo})$, to which the simulation predictions could be compared, but no such model exists for the ‘basic Co’ $d(\text{AlCoNi})$. However, the structure of the ‘W phase’ crystal approximant of ‘basic Co’ has been determined by Sugiyama *et al* [10], and we may apply what we have learned so far – in particular the period doubling and puckering – to predict its structure. [This study has inspired a more detailed modelling of W(AlCoNi), based on ab-initio energies rather than pair potentials [21].]

Using exactly the same tiles and interlayer spacing as in our other simulations, our unit cell is $23.25\text{\AA} \times 39.5606\text{\AA} \times 8.158\text{\AA}$, which differs by less than 1% from the experimentally determined lattice constants. The approximate atom content implied by Sugiyama’s structure solution and Co:Ni ratio is $\text{Al}_{385}\text{Co}_{113}\text{Ni}_{38}$, with uncertainties arising from the partial and mixed occupations. Adopting this composition as our ideal, we have $\text{Al}_{71.8}\text{Co}_{21.1}\text{Ni}_{7.1}$ at a density 0.0714 \AA^{-3} .

We applied our mock Hamiltonian from Sec. 3.2 to generate a tiling consistent with the $\tau^3 a_0$ binary rhombus tiling. The optimum configuration is unique (modulo symmetries) and has four 13\AA Ds, in an arrangement which turns out to be the same

as observed in $\text{W}(\text{AlCoNi})$. Cluster orientation comparisons were like performed like those of Subsec. 3.3, but using the relaxed energies (without MD). We found that, between the configurations with alternating and uniform cluster orientations, the latter had a lower relaxed energy, in accordance with the experimental W-AlCoNi structure. The atomic locations generated on this unit cell using the 4\AA rhombus decoration site list is approximately consistent with the experimentally determined sites.

Our MMC simulations are able to capture the gross features of W-AlCoNi with excellent accuracy. Since this approximant is not far from the ‘basic Co’ decagonal composition, we are not surprised to find $13\text{\AA}\text{Ds}$ and Star clusters as the major motifs, arranged in a manner consistent with our binary and τa_0 tilings, consistent with the observed W-phase. The differences in the exact atomic locations lie mainly within the highly context dependent 2.5th and 3rd rings. We find that the increase in density from our original simulations results in a more dense occupation of these rings. Atomic configurations found after RMR are in even better agreement. Fig. 2 compares one layer from experimental data to our RMR results; the match in the other layers are equally good.

However, a significant number of Al atoms in our RMR picture are in disagreement with the experimental refinement. because certain puckered atoms are not present in our simulations. The top right of Fig. 2 contains a pentagon of displaced Al atoms centred upon the missing Al atom. These extremely puckered Al atoms are perhaps located in energy minima too far away for our MD program to traverse. The existence of such atoms is one of the greatest flaws for beginning with a discrete site simulation.

5. Conclusion

We find that in the approximate composition $(\text{Al}_{70}\text{Ni}_{10}\text{Co}_{20})$, the structure of $d(\text{AlNiCo})$ is dominated by the formation of the $13\text{\AA}\text{D}$ clusters and the Star clusters which complement them. We find that the gross features are robust under variations of the composition and densities of $\sim 4\%$; these will strongly affect a few details of the sites and we have not established the correct answers for those atoms. Our method of tile decorations, and successive reductions of the degrees of freedom, affords an enormous speedup compared to brute-force molecular dynamics, which would get stuck in glassy configurations, at the price of a few plausible assumptions.

By applying our results to the approximant W-AlCoNi , we demonstrated both the validity and the pitfalls of our approach. The pitfall lies in that fact that our explorations are conducted using a fixed site list in two atomic layers, whereas the real structure has four layers and some atoms are strongly puckered out of them. Even though most puckered atoms may be represented as relaxations from ideal sites, the optimal puckered structure might be derived from a fixed-site structure of comparatively high energy that our simulations would pass over. Reliable answers can not be obtained by pure numerical exploration, but seem to demand some physical understanding of the puckering (and other displacements), as we have begun to do in Ref. [11]. The context dependences evident in the ‘basic Co’ show that

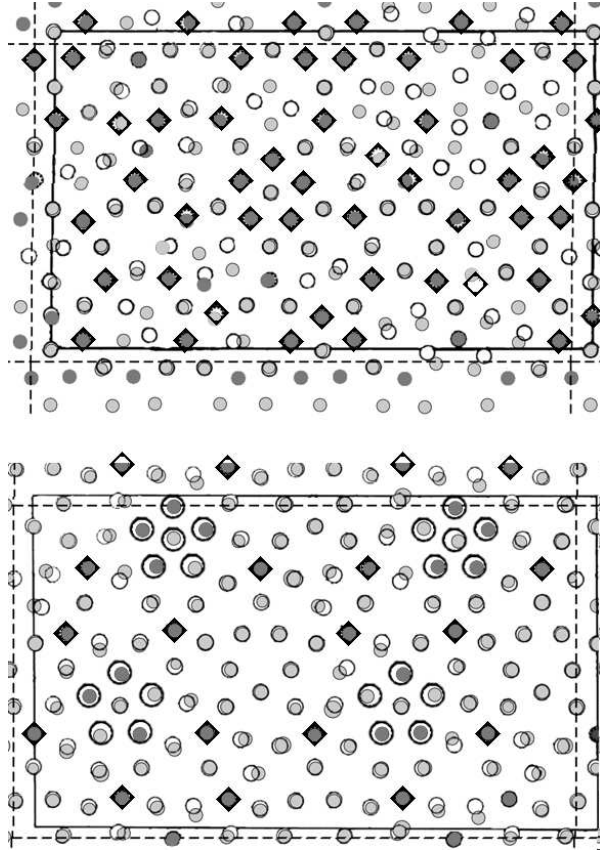


Figure 2. a) The top figure is one of the mirror layers of W-AlCoNi. b) The bottom figure is the puckered layer of W-AlCoNi. The empty circles are experimentally determined atom sites, the filled circles are those extracted from our simulations. Dark gray filled circles are TM, light gray filled circles are Al. Empty circles with 'teeth' are TM, smooth empty circles are Al. The large empty circles are experimental atomic sites with mixed Al-TM occupancies. The size of the simulated (filled) atoms may vary due to the visual scheme depicting distance in the c -axis dimension.

beyond a point, the errors in defining the pair potentials will surely exceed the energy differences due to some swaps of species, which is a second pitfall that may be alleviated only by checking against experimental phase diagrams.

Acknowledgments

This work is supported by DOE grant DE-FG02-89ER45405; computer facilities were provided by the Cornell Center for Materials Research under NSF grant DMR-0079992. MM was also supported by grant VEGA-2/5096/25 of the Slovak Academy

of Sciences. We thank M. Widom for discussions.

References

- [1] M. Mihalkovič, I. Al-Lehyani, E. Cockayne, C. L. Henley, N. Moghadam, J. A. Moriarty, Y. Wang, and M. Widom, Phys. Rev. B 65, 104205 (2002).
- [2] C. L. Henley, M. Mihalkovič, and M. Widom, J. All. Compd. 342 (1-2): 221 (2002).
- [3] M. Mihalkovič, C. L. Henley, and M. Widom, J. Non-Cyst. Sol. 334: 177 (2004).
- [4] S. Ritsch, C. Beeli, H. U. Nissen, T. Gödecke, M. Scheffer, and R. Lück, Phil. Mag. Lett., 74, (1996) 99-106
- [5] K. Edagawa, H. Tamaru, S. Yamaguchi, K. Suzuki, and S. Takeuchi, Phys. Rev. B 50, 12413 (1996).
- [6] B. Grushko, D. Hollard-Moritz, and K. Bickmann, J. All. Comp. 236, 243 (1996)
- [7] A. P. Tsai, A. Fujiwara, A. Inoue, and T. Masumoto, Phil. Mag. Lett. 74, 233 (1996).
- [8] S. Ritsch, C. Beeli, H. U. Nissen, T. Gödecke, M. Scheffer, and R. Lück, Phil. Mag. Lett. 78, 67-76 (1998). Philos. Mag. Lett. 78, 67 (1998)
- [9] B. Grushko, D. Hollard-Moritz, R. Wittmann, and G. Wilde, J. All. Comp. 280, 215 (1998).
- [10] K. Sugiyama, S. Nishimura, and K. Hiraga, J. Alloy Comp. 342, 65 (2002).
- [11] N. Gu, C. L. Henley, and M. Mihalkovič, Phil. Mag. 86, 593 (2006).
- [12] N. Gu, M. Mihalkovič, and C. L. Henley, preprint (www.arxiv.org: cond-mat/0602095)
- [13] J. A. Moriarty, and M. Widom, Phys. Rev. B 56 (1997) 7905-17.
- [14] M. Mihalkovič, W.-J. Zhu, C. L. Henley, and M. Oxborrow, Phys. Rev. B 53, 9002 (1996).
- [15] E. Cockayne and M. Widom, Philos. Mag. A 77, 593 (1998).
- [16] F. Lançon, L. Billard, and P. Chaudhari, Europhys. Lett. 2, 625 (1986).
- [17] M. Widom, K. J. Strandburg, and R. H. Swendsen, Phys. Rev. Lett. 58, 706 (1987).
- [18] C. L. Henley, p. 27 in *Quasicrystals*, ed. S. Takeuchi and T. Fujiwara (World Scientific, Singapore, 1998), available on archive cond-mat/9707326.
- [19] S. Ritsch, C. Beeli, and H.-U. Nissen, Phil. Mag. Lett. 74, 203 (1996).
- [20] X. Z. Li, R. C. Yu, K. H. Kuo, and K. Hiraga, Phil. Mag. Lett. 73, 255 (1996).
- [21] M. Mihalkovič and M. Widom, Phil. Mag. 86, 557 (2006).